Bulletin of Earthquake Engineering
https://doi.org/10.1007/s10518-024-02055-z

ORIGINAL ARTICLE

Advanced nonlinear soil-structure interaction model for the seismic analysis of safety-related nuclear structures

J. M. Gonzalez[1,2] · A. H. Barbat[1,2] · Y. F. Vargas-Alzate[1] · F. Rastellini[1,2] · J. Ramirez[1,2] · C. Escudero[2] · L. G. Pujades[1]

Received: 27 May 2024 / Accepted: 19 October 2024
© The Author(s) 2024

Abstract
This article proposes an advanced nonlinear soil-structure interaction methodology, for the seismic analysis of a nuclear structure. To do so, a study is performed on a nuclear reinforced concrete structure considering the effects of the nonlinearity due to the sliding and rocking at the soil-structure interface, under a *Beyond Design Basis Earthquake*. A tridimensional numerical model based on the Finite Element Method is developed for the structure and the soil. The model of the structure considers composite materials to describe all the structural members, taking full advantage of the modelling capabilities of the finite element method. The soil layers are modelled assuming their degraded properties due to the propagation of the seismic ground motion. An innovative approach to achieve spectral matching at the surface of the FEM soil model after propagation from the bedrock has been successfully implemented. The seismic analysis on the structure has been performed by considering three hypotheses for the contact between soil and structure: fixed-base, fixed contact and sliding-rocking contact. Insights are provided after comparing floor spectra for the contact approaches assessed in this research, calculated at the systems and components' locations at the nuclear structure. Finally, a statistical approach for the soil properties allows to study the effects of these uncertainties on the structural response.

Keywords Nuclear structure · Soil-structure interaction · Floor spectra · Wave propagation

1 Introduction

Climate change is forging a new era in which nuclear energy play an important role. It is because the current need of energy with zero carbon emissions is increasing. However, due to the very harmful consequences of nuclear accidents on the environment, special attention must be paid to the safety of these structures against natural hazards, NHs. Regarding earthquakes, accidents such as the one at the Fukushima power plant (Koo et al., 2014) have called into question the safety of these structures (Coleman et al., 2016). As a consequence, on March 24, 2011, the European Council agreed to carry out a plan to subject all Euro-

Extended author information available on the last page of the article

Published online: 12 November 2024

pean nuclear power plants to a homogeneous set of "tests" that would allow assessing their capacity to withstand situations beyond their design bases and identify the existing safety margins, as well as the possible measures that could be implemented to improve their security. To do so, cutting-edge methodologies must be considering in the modelling process to properly estimate these capacity and safety margins.

The seismic analysis of nuclear structures involves many complex issues related to the structural behavior, modelling techniques or definition of the seismic ground motions. In the latter respect, the *Design Basis Earthquakes* (DBE) are used to establish the acceptable performance requirements of the structures, systems, and components, such that a nuclear power plant can withstand the event and not endanger the health or safety of the plant operators or the wider public. Events like the Fukushima earthquake and other earthquakes stronger than the corresponding to the design basis, evidenced the need to go further in the design and evaluation stage, and increase the earthquake demand for the evaluations of seismic hazards for nuclear structures. Beyond Design Basis Earthquakes (BDBE) became increasingly important as a reference for seismic analysis. In this context, contact nonlinearity at the soil-structure interface becomes determinant in the computation of the seismic response of the structures. As consequence, efforts have also been made to incorporate nonlinearities into the codes and standards (Coleman et al., 2016).

In terms of modelling the seismic response of a structure under seismic motions, some remarkable works can be highlighted. Bolisetti et al. (2014, 2015) benchmarked the time-domain calculation methods of the soil-structure interaction against the frequency domain methods for a number of sites, given linear and nonlinear response. Hashemi et al. (2015) developed analysis techniques to improve the seismic design and discussed the effects of structural nonlinearities on the shear walls of a nuclear structure and the geometric nonlinearity at the soil-structure interface. The study was performed using the so-called *stick model* defined as a simplification of a FE model, where the shear walls are represented by beams. Coleman et al. (2016) developed a framework for the time-domain nonlinear SSI analysis. Recommendations for the numerical methods and codes to be employed, for modelling the soil and structural domains, requirements for the mesh or the time step to ensure the stability are given in this framework to finally enumerate a set of verifications to ensure the reliability of the results. Datta et al. (2017) investigated the effects of nonlinearities at the soil-structure interface on the peak acceleration demands, taking as reference the seismic ground motion data and site soil profile near the Fukushima Daichii nuclear power plant.

In line with the above, this article presents a series of integrated methodologies oriented to properly estimate seismic effects for nuclear structures, which is a key aspect to achieve the objective faced not only by European countries but also globally. To do so, it has been analyzed the dynamic response of an existing reinforced concrete nuclear structure subjected to seismic ground motions. Amongst many other innovative aspects developed within this research, the nonlinear effects due to sliding and rocking at the soil-structure contact interface has been analyzed and compared with a fixed-base model. A finite element method (FEM) based model, considering relevant aspects of the dynamic response of the combined system (Soil+Nuclear building), has been developed. All the structural members of the nuclear building like shear walls, slabs, beams and columns are modelled as composite materials considering the different behavior of concrete and steel, to improve the structural solution obtained. This approach entails a new step in modelling the soil-structure interaction (SSI) problem. The foundation of the building and a lean concrete layer are also mod-

elled to properly represent the dynamic response of the system. In addition, the numerical model includes the interaction with the underlying soil layers to fully reproduce its influence upon the structural response when a set of BDBE seismic ground motions, which have been fitted to a given target spectrum, is applied at the bedrock.

In order to characterize the free-field motion, it has been employed an advanced procedure, recently presented in Vargas-Alzate et al. (2024), to perform spectral matching when considering FEM representations of a soil volume. It is worth mentioning that, due to the wide safety margins considered in the design of a nuclear building, non-linear behavior of the structural elements is not to be expected, as in the case of normal structures. For this reason, linear behavior is assumed for the structural materials, that is, concrete and steel. In the case of soil, since the shear strains observed do not exceed extreme values (higher than 0.4%), the equivalent linear analysis has been employed to model the nonlinear behavior of the soil (Yoshida et al. 2002). Regarding the sliding and rocking at the soil-structure interface, three soil-structure contact hypotheses are considered to evaluate the behavior of the structure.

Therefore, since inelastic behavior of the structural elements is unlikely, this article has focused on the calculation of *in-structure response spectra* (ISRS) at different locations, also known as floor spectra (Ahn and Park, 2022). The floor spectra are used as an indicator to verify the adequate performance of the safety-related systems and components. The study is completed with a statistical approach to consider the uncertainty of the soil mechanical properties and its effect on the structural response. This paper includes results for all these challenging issues and the corresponding conclusions.

2 Global soil-structure model

The numerical model developed for this study involves the definition of the FEM model for both the structure and the soil, with a soil-structure interface in between. The features and development of the soil-structure FEM model are detailed in this section.

2.1 FEM model of the structure

An existing reinforced concrete structure from a nuclear plant has been studied herein. The structure is categorized as Seismic Class 1 (ASCE, 2017; US NRC Regulatory Guide 1.29, 2021) according to its functionality. The plan view of the building shows a rectangular-like shape, 64,4 m long and 61,9 m wide, with a semicircular cut with radius 22,5 m trimmed on one of its sides, corresponding to the adjacent containment building. The building presents a symmetry plane in the y (longitudinal) direction; the orthogonal plane is the x (or transversal) direction as depicted in Fig. 1. The foundation level is at the elevation + 91.00. The building has one intermediate floor at elevation + 96.00, three floors at elevations + 100.00, + 108.00 and + 114.50, and a roof at elevation + 120.70 (Fig. 1). The structure is composed of several structural members: slabs, shear walls, beams and columns with a wide range of dimensions. Figure 2 shows the details of floors + 91.00 and + 96.00 (a) and floor + 114.50 (b), where the structural members can be appreciated.

The structure has been modelled with *rotation-free 3-node shell elements* (Flores et al. 2005). This element shows a good performance for the bending behavior of the structure as

Fig. 1 Geometrical definition of the nuclear structure (**a**) top view (**b**) elevation view

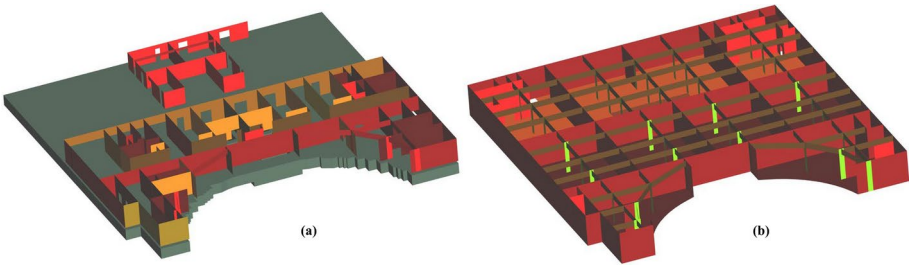

Fig. 2 Structural model for the nuclear structure. (**a**) floors + 91.00/ + 96.00 (**b**) floor + 114.50

well as the capacity of being assembled with solid elements, like the hexahedral elements used to model the foundation. The shell element incorporates a composite definition of the reinforced concrete members. The overall behavior of the composite material is obtained by applying the mixing theory. In the Authors' knowledge, this kind of elements have not been used before in SSI analysis.

The foundation of the structure is a reinforced concrete slab of 61.0×63.6 m in plant and 2 m thick. It is modelled with a structured mesh of 8-node linear hexahedra. This mesh is consistently joint to the shell elements used to discretize the structure through rotation-rigid links to ensure the rigid rotation of the joint, since the finite elements involved only have translational degrees of freedom. This link is performed by a master–slave condition between the solid and the shell elements to enforce that the relative rotation is null. The foundation is supported on a lean concrete layer with similar dimensions, 63.0×65.6 m, which is modelled assuming a uniform thickness of 4 m. This special layer has also been discretized using a structured mesh of 8-node linear hexahedra. All the structural parts of the nuclear building are assumed to behave within the elastic range. The material properties for building concrete and steel are briefly described in Table 1.

The 3D numerical model assumes a viscous damping model, where the damping forces are related to the velocity at the calculation points, which simplifies the calculation. Further details can be found at (Martinez et al., 2011) As long as the time step for the calculation process with an explicit time integration scheme depends on the minimum size of the finite elements, and this is expected to occur in the structural model, a sensitivity analysis has been performed on the mesh of the structure to optimize the computational cost of the simu-

Table 1 Material properties of the structural elements in the nuclear structure

	Structural concrete	Structural Steel	Foundation concrete	Lean concrete
Density (kg/m^3)	2400	7850	2500	2300
Young Modulus (GPa)	28.7	210.0	28.7	18.1
Poison coefficient	0.20	0.30	0.20	0.17

Table 2 Modal analysis of the structure

Mode	Transversal direction (x)			Longitudinal direction (y)		
	Frequency (Hz)	Period (s)	Mass part. Factor (%)	Frequency (Hz)	Period (s)	Mass part. Factor (%)
1	8.2	0.1214	49.9	8.5	0.1176	50.7
2	8.5	0.1176	15.9	8.2	0.1214	13.0
3	10.2	0.098	7.3	10.9	0.0915	7.4
4	17.2	0.0581	2.4	17.2	0.0581	1.1
5	17.6	0.0568	1.2	10.2	0.098	0.9

lation. Accordingly, the minimum size of the shell elements is 34 cm, which ensures the stability of the simulation with reasonable computational cost. Therefore, the structural model is composed of 324,150 3-node shell elements while the foundation and the lean concrete layer are composed of 59,796 8-node linear hexahedral elements.

A modal analysis of the structure has been performed considering the dynamic character of the problem. The natural frequencies and the corresponding mass participation factors for x,y directions are summarized in Table 2.

2.2 FEM model of the soil

For the soil column definition, a soil profile is available from a geotechnical study. This profile shows a multilayered scheme with ten strata, where the bedrock is identified as the depth where a shear wave velocity is higher than 2500 m/s. This condition leads to a model with a depth of 198.30 m. This depth is slightly higher than three times the width of the foundation of the structure, which is a recommendation given by ASCE (2017). The mechanical properties are obtained from the aforementioned basic soil profile as will be explained in Sect. 4. The horizontal dimensions of the soil model are chosen according to the requirements for the lateral boundaries found in ASCE (2017) to reproduce the real dynamic behavior, that is, the boundaries must be far enough from the structure so that "*the effect of the waves reflected by the boundary is somewhat small when reaching the structure and thus does not significantly affect the seismic response*". This requirement is complemented with cyclic symmetry conditions at the lateral surfaces of the soil. After some analyses, the requirement for the reflection of the waves is accomplished with a square soil model of 630 m per side, which means a soil/structure width relation around 10.

The soil domain has been meshed by 1,43 M 8-node linear hexahedral finite elements. The sizes of the soil elements have been chosen taking into account its capability to reproduce the dynamic response, avoiding to filter high frequencies (ASCE, 2017). The size of the finite elements assures that the vertical propagation of the ground motion is able to reproduce a maximum frequency f^{max}, for the shear wave velocity of every soil layer. This

leads to a maximum element size for each layer (h_i^{max}) calculated as $Vs_i/5f^{max}$, where Vs is the shear wave velocity; $f^{max}=100$ Hz has been chosen as maximum frequency. This upper limit is beyond the expected frequency content of the seismic ground motions. Yet, according to ASCE 2017 paragraph C3.1, in-floor spectra should be calculated to cover a frequency range up to 100 Hz. Although this assumption increases the computational effort, f^{max} has been set at 100 Hz to ensure that the model do not filter high frequency waves. Consequently, the vertical sizes vary according to the shear wave velocity from the smaller elements (2.20 m) at surface level, to the largest (3,40 m) in the sixth layer.

2.3 Soil-structure contact interface

The interface between the structure and the soil models has a crucial effect on the dynamic analysis. The soil-structure contact interface is located between the lean concrete layer and the first soil layer, where a contact model is defined between the two surfaces. Various numerical methods have been proposed in the literature to deal with the contact problem at an interface. Among them, the penalty methods, Lagrange multiplier methods, the augmented Lagrangian approach and the Nitsche method can be mentioned. Dawson et al. (1995) used a consistent penalty method to model the metal forming process. Fischer et al. (2005, 2006) used penalty methods to solve 2D frictional contact problems for large deformations. Oliver et al. (2009) and Weyler et al. (2012) propose a methodology called *Contact Domain Method*, where the Lagrange or the penalty approaches are used. Although methods based on Lagrange multipliers directly and exactly enforce the contact constraint, they present the difficulty of the need to introduce extra variables, which expands the system of equations and modify the stiffness matrix of the problem.

The penalty method is very convenient when using an explicit scheme to perform the time integration of the dynamic equations. Hence, this penalty method is the chosen algorithm for the simulation of the soil-structure contact problem in this paper. To take into account the friction, a Coulomb model that establishes the starting threshold from which tangential slip occurs, is used. A friction coefficient of 0,5 is assumed in this study for the sliding contact surface. Figure 3 shows a scheme of the contact interface of the numerical model.

The nuclear structure is surrounded by different adjacent buildings. The adjacent buildings are separated from the analyzed building by means of joints or separation gaps. Accordingly, the possible frictional or hammering interactions with adjacent buildings are neglected. The lateral restriction produced by the surrounding soil is modelled by apply-

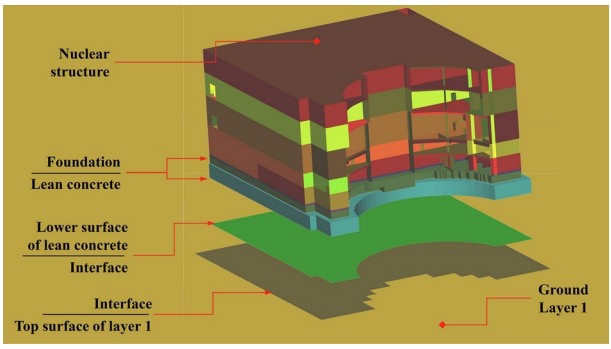

Fig. 3 Model of soil-structure contact interface

ing an elastic restraint that replicates the movements of the upper layer of the soil. Elastic springs around the entire perimeter of the building are placed to reproduce the effect of the lateral confinement exerted by the soil on the structure. The stiffness of the horizontal springs is established based on the ballast coefficient corresponding to the surrounding soil. A soil ballast coefficient of 40 MN/m^3 is used in the contact model, which can be considered a conservative value for the existing soil type.

2.4 Global soil-structure FEM model

The structural and soil FEM models, the contact algorithm and the boundary conditions define the global model for the soil-structure interaction problem of the nuclear structure. Figure 4 shows a general view of the global FEM model and that of the structural model. Two different types of boundary conditions are considered for the global model. The soil layers are supported on the bedrock and, consequently, the displacements are prescribed at the bottom surface of the model where the bedrock is found. Cyclic symmetry conditions are applied at the lateral surfaces of the soil model. This condition is implemented by linking opposite vertical surfaces to enforce the same response in terms of displacements, velocities and accelerations. This is equivalent to prescribe periodic conditions to the model to minimize the reflection of the waves, as explained in Galindo et al. (1993).

The soil-structure interaction problem has been solved using a FEM-based code named PLCD.[1] This code can solve structural dynamic problems with several constitutive material formulations and finite element typologies like 2D elements, beams, shells or 3D solids, involving composites discretization and solutions based on the rule of mixtures theory (Rastellini et al., 2008); it has also implemented several contact models. The solution of the soil-structure problem has been performed in the time domain using an explicit time-integration scheme with a time step of $0.23 \cdot 10^{-3}$ s. This time step is obtained from the finite element mesh, considering the minimum size, to guarantee the stability of the calculation process. The capabilities and accuracy of PLCD explicit code for structural analysis of nuclear structures has been specifically validated from experimental benchmarks (Jimenez et al., 2021)

[1] PLCD home page: https://www.cimne.com/PLCD

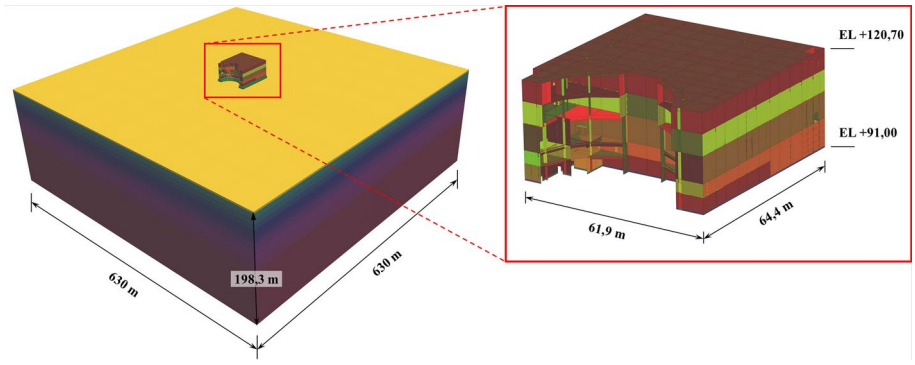

Fig. 4 Global model and detail of the nuclear structure

Table 3 Mechanical properties of the soil column at low shear strains

Layer	Thickness (m)	Vs (m/s)	Damping (%)	Density (kg/m^3)	Shear modulus (GPa)	Young modulus (GPa)	Poisson (-)
1	3.32	1098	3.0	2203.1	2,7	7,2	0.36
2	9.00	1119	3.0	2208.2	2,8	7,5	0.36
3	9.00	1142	3.0	2213.7	2,9	7,9	0.37
4	9.00	1111	3.0	2206.2	2,7	7,5	0.37
5	14.00	1660	2.4	2326.0	6,4	17,4	0.36
6	8.00	1643	2.4	2322.6	6,3	17,1	0.36
7	12.00	1695	2.4	2333.1	6,7	18,2	0.36
8	22.00	1175	2.9	2221.3	3,1	8,4	0.37
9	16.00	1175	2.9	2221.3	3,1	8,4	0.37
10	96.00	1575	2.5	2308.5	5,7	15,8	0.38

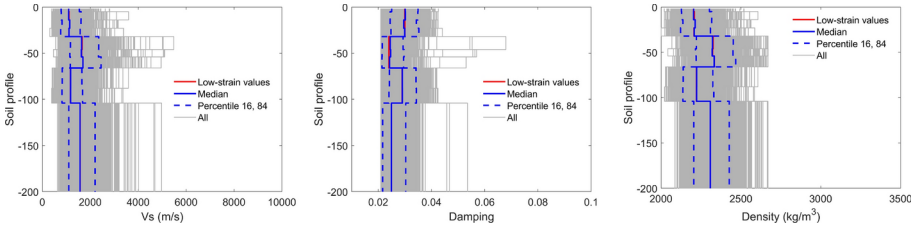

Fig. 5 Probabilistic soil profiles for low shear strains

and widely used in similar works related to structural analysis of nuclear structures (Cornejo et al., 2018) and composite structures (Barbu et al., 2019).

3 Probabilistic characterization of the soil profiles

The geotechnical information about the building site is limited, and so, uncertainties for the mechanical properties of the soil layers should be considered. To do so, a statistical study has been performed over the basic soil profile available. Table 3 summarizes the mechanical properties of this profile for low shear strains. From this basic profile, 1000 probabilistic soil profiles have been generated considering that 1) the shear wave velocity (Vs) follows a log-normal distribution with a median value equal to the basic profile and a logarithmic deviation of 0,35 all along the profile, and 2) the velocity of the shear waves in the different layers are correlated according to the Toro's model (Toro, 1996). It should be noted that 1000 profiles have been generated, instead of the 60 suggested by the various reference standards provided, in order to reduce statistical variability in the estimation of percentiles. Figure 5 shows the generated soil profiles.

3.1 Definition of seed signals

For guidelines requirements, this study has considered a set of seven seismic ground motions, which has been selected and modified to be compatible with a *Beyond Design Basis Earthquake (BDBE)*. Horizontal and vertical UHS are available for the BDBE at foun-

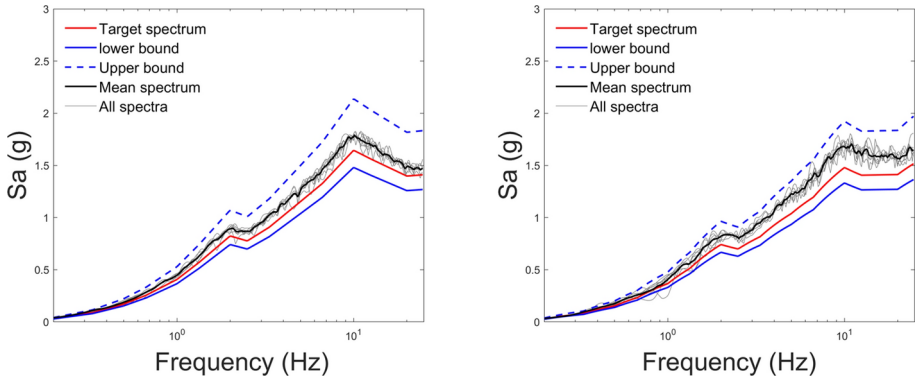

Fig. 6 Target spectra and spectrally matched signals. **a** horizontal component (**b**) vertical component

Table 4 Mechanical properties of the *Upper Bound* (UB) soil column after propagation

Layer	Thickness (m)	Vs (m/s)	Damping (%)	Density (kg/m^3)	Shear modulus (GPa)	Young modulus (GPa)	Poisson (-)
1	3.32	1540.3	3.15	2302.6	5.5	14.9	0.36
2	9.00	1590.0	3.72	2317.0	5.9	15.9	0.36
3	9.00	1571.0	3.96	2316.6	5.7	15.7	0.37
4	9.00	1515.7	4.28	2309.3	5.3	14.5	0.37
5	14.00	2341.2	2.87	2451.9	13.4	36.6	0.36
6	8.00	2316.8	2.96	2450.1	13.2	35.8	0.36
7	12.00	2421.0	3.00	2467.2	14.5	39.3	0.36
8	22.00	1574.5	4.27	2324.2	5.8	15.8	0.37
9	16.00	1578.5	4.62	2329.9	5.8	15.9	0.37
10	96.00	2089.1	4.04	2426.7	10.6	29.2	0.38

Table 5 Mechanical properties of the *Best Estimate* (BE) soil column after propagation

Layer	Thickness (m)	Vs (m/s)	Damping (%)	Density (kg/m^3)	Shear modulus (GPa)	Young modulus (GPa)	Poisson (-)
1	3.32	1090.9	3.36	2203.1	2.6	7.1	0.36
2	9.00	1051.4	4.50	2208.2	2.4	6.6	0.36
3	9.00	1065.9	5.10	2213.7	2.5	6.9	0.37
4	9.00	996.2	6.10	2206.2	2.2	6.0	0.37
5	14.00	1597.9	3.47	2326.0	5.9	16.2	0.36
6	8.00	1558.1	3.78	2322.6	5.6	15.3	0.36
7	12.00	1620.0	3.88	2333.1	6.1	16.7	0.36
8	22.00	1068.2	5.74	2221.3	2.5	6.9	0.37
9	16.00	1054.1	6.08	2221.3	2.5	6.8	0.37
10	96.00	1418.5	5.37	2308.5	4.6	12.8	0.38

dation level (See red line in Fig. 6); they have been derived from a PSHA (Cornell, 1968). The vertical component has been obtained applying the Table 4–5 from NUREG/CR-6728 (2001). According to this study, earthquakes compatible with this seismic scenario have a magnitude and a distance from the source of 6.3 and 2.0 km, respectively.

As a first step, a selection of the as-recorded acceleration time histories (*seed signals*) is performed from the *Pacific Earthquake Research Center (PEER)*.[2] This database provides time-history records of acceleration for three orthogonal components (Two horizontal and one vertical) according to the seismic parameters (magnitude, distance and target spectrum) of the building site. In this manner, a family of seven acceleration time histories in three directions {x, y, z} has been defined to take into account the variability and uncertainty of the expected ground motion. These seed signals have been then adjusted using a spectral matching technique that modifies their frequency content in such a way that the resulting ground motion approaches the aforementioned target spectra; *SeismoMatch*[3] software has been used to this end. This program is based on the wavelets algorithm proposed by Abrahamson (1992) and Hancock et al. (2006). Satisfactory adjustments to the objective spectrum have been obtained, for all the accelerograms, according to the requirements provided by the Appendix F of RG 1.208 (USNRC, 2007) and Sect. 3.7.1 from USNRC (2014). Figure 6 depicts the mean spectrums for the horizontal and vertical components of the adjusted ground motions, over the target spectra for the building site, with the upper and lower admissible limits prescribed by RG 1.208 appendix F, items 3 and 4. In the case of the horizontal component (Fig. 6, left), the spectra shown are the geometric mean of the horizontal spectra.

3.2 Degradation of the soil profiles

The generated profiles shown in Fig. 5 represent dynamic properties for low shear strains which means, they are elastic profiles. However, in case of earthquakes with high magnitude, it is quite likely that the mechanical properties of the soil profiles for low shear strains change after propagation. In order to consider this nonlinear effect, the *Equivalent Linear Method* (ELM) (Seed and Idriss, 1970) has been employed in this research. For the application of this method, one of the adjusted signals, whose spectra have been presented in Fig. 6, has been employed. Note that this signal is assumed at the surface of the soil model, therefore, to estimate the degradation of soil mechanical properties, the procedure used to estimate the time-history evolution at the interfaces is deconvolution (Poul and Zerva, 2018). This signal has been employed to estimate the degradation of the material properties of the one thousand soil profiles at layer level. The degradation of the dynamic properties of the soil have been performed by means of the secant shear modulus normalized, G/G^{max}, and hysteretic damping curves with the shear strain for firm rock found at EPRI (2013) reproduced in Fig. 7 for convenience.

From the resulting properties, three different soil profiles have been defined: Lower Bound (LB), Best Estimate (BE) and Upper Bound (UB), corresponding to percentiles 16%, 50% and 84%, respectively, for every material property, calculated at layer level. These three profiles are defined by the shear wave velocity (Vs), density (ρ) and damping ratio (ξ). This procedure has been applied using the software *DEEPSOIL* (Hashash et al. 2020). Figure 8 shows the degraded samples for the soil columns and highlights the three soil columns considered {LB, BE, UB} and Table 4 to Table 6 detail their mechanical properties after the deconvolution procedure. Considering that the shear strains observed show values

[2] PEER database web site: https://ngawest2.berkeley.edu/ (last access 04/07/2021).

[3] https://seismosoft.com/products/seismomatch

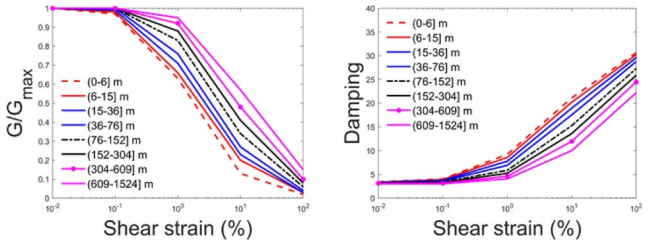

Fig. 7 G/G^{max} and hysteretic damping as a function of the shear strain for firm rock

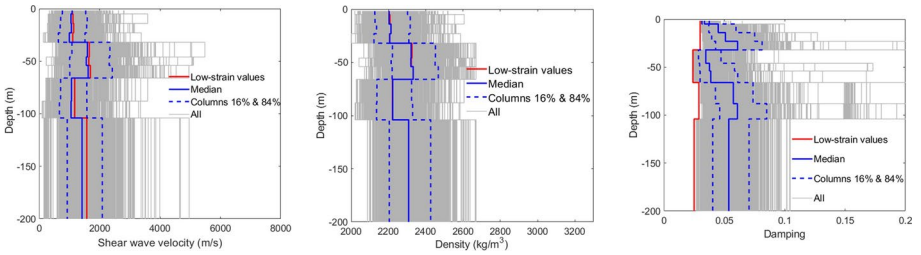

Fig. 8 Statistical treatment of the soil columns mechanical properties

Table 6 Mechanical properties of the *Lower Bound* (LB) soil column after propagation

Layer	Thickness (m)	Vs (m/s)	Damping (%)	Density (kg/m^3)	Shear modulus (GPa)	Young modulus (GPa)	Poisson (-)
1	3.32	769.4	3.76	2126.8	1.3	3.4	0.36
2	9.00	712.7	5.97	2128.1	1.1	2.9	0.36
3	9.00	693.8	7.51	2136.5	1.0	2.8	0.37
4	9.00	635.3	8.13	2122.3	0.9	2.3	0.37
5	14.00	1083.5	4.73	2221.4	2.6	7.1	0.36
6	8.00	1009.8	5.85	2214.8	2.3	6.1	0.36
7	12.00	1014.2	6.11	2219.9	2.3	6.2	0.36
8	22.00	709.7	7.38	2138.5	1.1	3.0	0.37
9	16.00	669.9	8.51	2136.2	1.0	2.6	0.37
10	96.00	928.5	7.05	2204.6	1.9	5.2	0.38

around 0.005%, with maximum significant values around 0.02% (See Fig. 9), the use of ELM can be justified according to Kaklamanos (2013). More details about this procedure can be found in Vargas-Alzate et al. (2024).

4 Seismic ground motions

The BE soil column summarized in Table 4 has been used to define the degraded soil profile. Then, the set of seven records, spectrally matched in the previous section (See Fig. 6), have been deconvoluted through this soil profile. The resulting signals are then applied at the base of the 3D-slice model to verify the compatibility with the target spectra at the soil

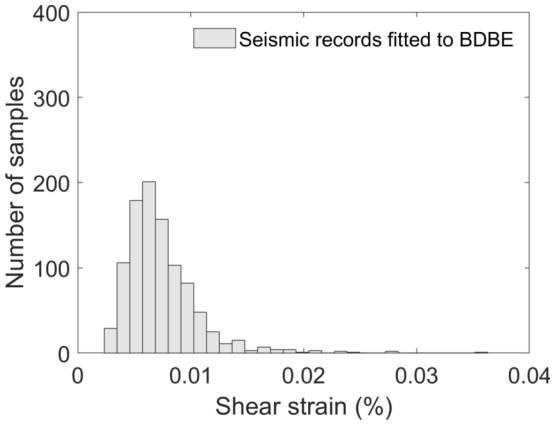

Fig. 9 Maximum shear strains reached after applying ELM

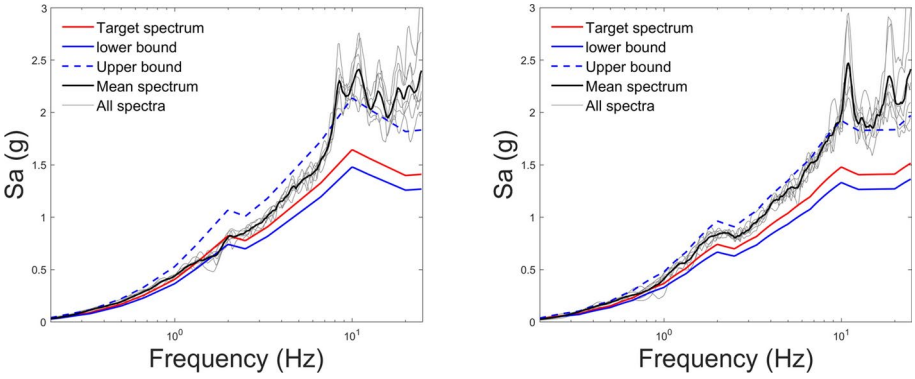

Fig. 10 Target spectra at the surface using the deconvoluted signals at the base of the 3D-slice FEM model. **a** horizontal component (**b**) vertical component

surface according to US NRC Regulatory Guide 1.208, appendix F. Figure 10 shows these verifications for the BDBE records. It can be seen that the upper and lower limits cannot be met without further modifications of the original deconvoluted signals. This incompatibility obeys to the limitations of the 1D deconvolution model that are overcome with the 3D-slice model like the simultaneity of the horizontal and vertical components or the Poisson's effect.

In order to better approximate the expected soil surface response of the FEM model, the procedure presented in Vargas-Alzate et al. (2024) has been employed. In brief, these authors propose to create an enhanced transfer function, which is a linear combination of the transfer functions from both the 1D and the 3D models. The latter can be estimated as the ratio between the amplitude response spectra of both the surface and base signal. Based on this innovative approach, the spectra of the resulting signals at the surface of the 3D-slice model approximate much better the target spectrum, as it can be seen in Fig. 11.

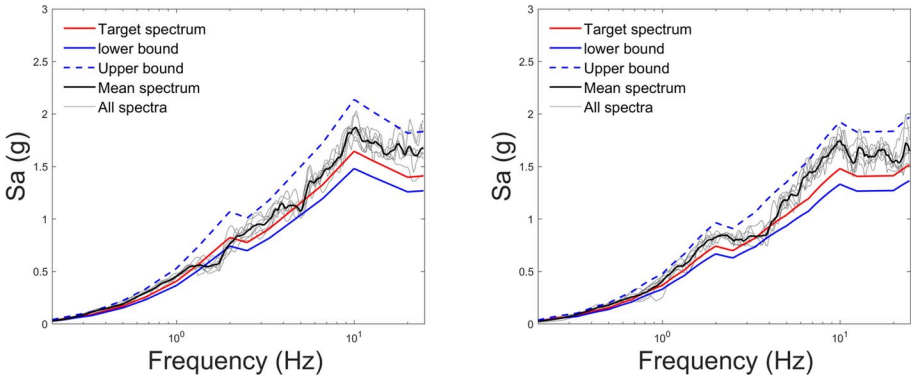

Fig. 11 Target spectra at the surface after applying the procedure proposed in Vargas-Alzate et al. (2024). **a** horizontal component (**b**) vertical component

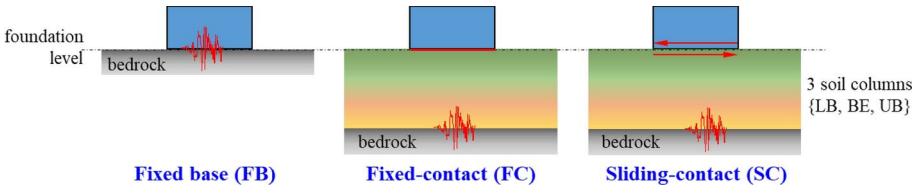

Fig. 12 Soil-structure contact hypotheses

5 Seismic analysis of the soil-structure model

Once the free-field response of the 3D FEM model has been properly characterized (See Fig. 11), the signals that act at the base of this model can be used to study the SSI problem. By considering the full model (i.e., building and soil), the simulation of the seismic problem requires a significant computational effort. Every case has been executed in an HPC workstation, delivered in 12 cores of 64 GB RAM capacity, requiring a variable time from 48 to 72 h, depending on the ground motion duration. The results of the numerical simulation have been postprocessed by means of the GiD Pre-Post Processor developed by CIMNE.[4]

Three contact hypotheses for the soil-structure interface are considered in the analysis: 1) the structure supported on a rigid base without soil interaction (fixed base, FB); 2) a soil-structure model with a fixed contact, where neither sliding nor rocking are produced at the interface, although the soil interacts with the structure (fixed contact, FC); and 3) a contact interface between the structure and the soil where sliding and rocking are allowed (sliding contact, SC). Figure 12 shows the three contact hypotheses considered herein.

The numerical simulation of the earthquake is performed by applying the seismic ground motion at the bedrock level. Time histories of acceleration, velocities and displacements are obtained and postprocessed at the end of the seismic motion.

The structural response of the nuclear building is evaluated for the three soil-structure contact hypotheses {FB, FC, SC} in terms of floor spectra. The evolution of the seismic response along the height of the building is analyzed by means of the floor spectra at three

[4] GiD home page: www.gidsimulation.com

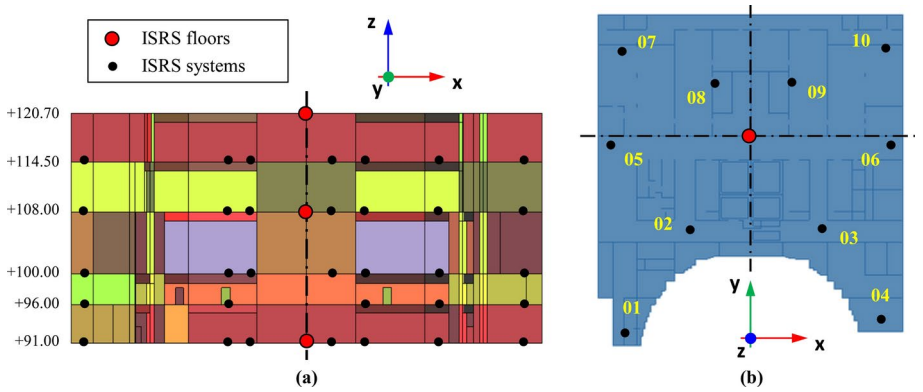

Fig. 13 Locations of the calculation points for the floor spectra

Table 7 Input and output variables of the study

Input/output variables	Items
Ground motions	7 seismic ground motions
Soil contact hypotheses	Fixed base (FB), Fixed-contact (FC), Sliding-contact (SC)
Soil columns	Lower Bound (LB), Best Estimate (BE), Upper Bound (UB)
Floor spectra	3 calculation points at three floor levels 46 calculation points at locations of the systems and components

floor levels. On the one hand, these floor spectra are obtained in vertical line in the intersection of the symmetry plane (*yz*) and an existing shear wall parallel to *xz* plane, continuous through the height of the building. On the other hand, floor spectra are also calculated at the locations of the non-structural components related to the operation and safety tasks of the nuclear building, that is 46 calculation points distributed in the five floors (ten points/floor with six additional points in the intermediate level). All the floor spectra for the structural response of the building are calculated for the *BE* soil column.

Additionally, the effects of the uncertainty about the soil mechanical properties are also studied to analyze its effect over the seismic response. The influence of the three soil columns {LB, BE, UB}, defined in Sect. 3, on the floor spectra are analyzed at the foundation and the roof level. Figure 13 shows a scheme of the location of the calculation points for the in-structure response spectra, which in this study are actually, floor spectra: (a) shows a lateral view with the elevations of the calculation points while (b) shows the location of the calculation points in a single floor, which is replicated in the rest. Table 7 shows a summary of the input variables, ground motions and soil columns, and locations of the floor spectra as output results. All the floor spectra are calculated as the median of the results obtained from the seven ground motions considered, given a 5% damping ratio.

6 Results

6.1 Effect of the sliding-rocking on the floor spectra

When a seismic wave propagates from one soil layer to another, it experiments reflection/refraction and variation of the propagation velocity. This fact is the responsible of two effects that potentially determine the overall response of the soil-structure system: 1) the free-field motion is modified by the presence of both, the structure and the characteristics of the interface. This effect is known as *kinematic interaction*. 2) The dynamic response of the structure due to the seismic ground motion produces a deformation in the underlying soil domain; this effect is known as *inertial interaction* (Davoodi et al., 2015). Both effects are studied by means of free-field response spectra and of floor spectra at different locations of the structure, which are used as indicators of the structural behavior due to the propagation of the seismic motion from the bedrock up to the roof level of the structure.

The effects of the contact interface are analyzed by means of two sets of results shown in this section: (1) the variation of the floor spectra along a vertical axis located in the center of the building; (2) the floor spectra obtained at the 46 predefined points, where systems and components are located within the nuclear structure. In all cases, the effects of the soil-structure contact interface are evaluated in function of the variation of the peak acceleration of the floor spectra (PSA) and the associated peak frequency (f^{PSA}). Figure 14 shows the floor spectra for the three directions {x, y, z} in the rows, and three contact hypotheses {FB, FC, SC} in the columns. In this figure, spectra are shown at the soil surface for the free-field case (FF) and the floor spectra are given at three floor levels: foundation level (+91.00), an intermediate story (+108.00) and roof level (+120.70). Table 8 summarizes the PSA and f^{PSA} values obtained.

The effect of the structure on the free-field response and the propagation of the ground motions through the structure are analyzed by calculating the evolution of PSA and f^{PSA} ratios with respect to a reference for the three contact interface cases. The effect of the structure on the response spectra at surface level is analyzed comparing the floor spectra at the foundation level with the free-field response spectra. The ratio of PSA at the foundation level to the PSA for the free-field response is denominated π_{FF}. Table 9 shows the PSA ratios (π_{FF}) for the three soil-structure contact hypotheses.

The evolution of the seismic response along the structure is measured in terms of the ratio of PSA at the roof level to the PSA at the foundation level. This ratio is denominated π_{RF}. Table 10 shows the PSA ratio π_{RF} for the three soil-structure contact hypotheses. The evolution of the PSA ratios, π_{FF} and π_{RF}, with the contact interface case are graphically represented in Fig. 15.

The main natural frequency of the structure, according to the modal analysis, is around 8.2–8.5 Hz with a mass participation factor around 65%. As a general observation, the influence of the soil and of the soil-structure contact interface leads to a flattening of the floor spectra and a reduction of the range of frequencies in the response spectra.

At surface level, the free-field response spectra show a wider range of frequencies. The floor spectra at the foundation show a decrease in the range of frequencies with respect to the free-field spectra as the contact at the interface becomes more flexible and movements at the contact interface develop. This decrease affects especially to the high frequencies range, which highlights the relevance of the nonlinearity in the analysis.

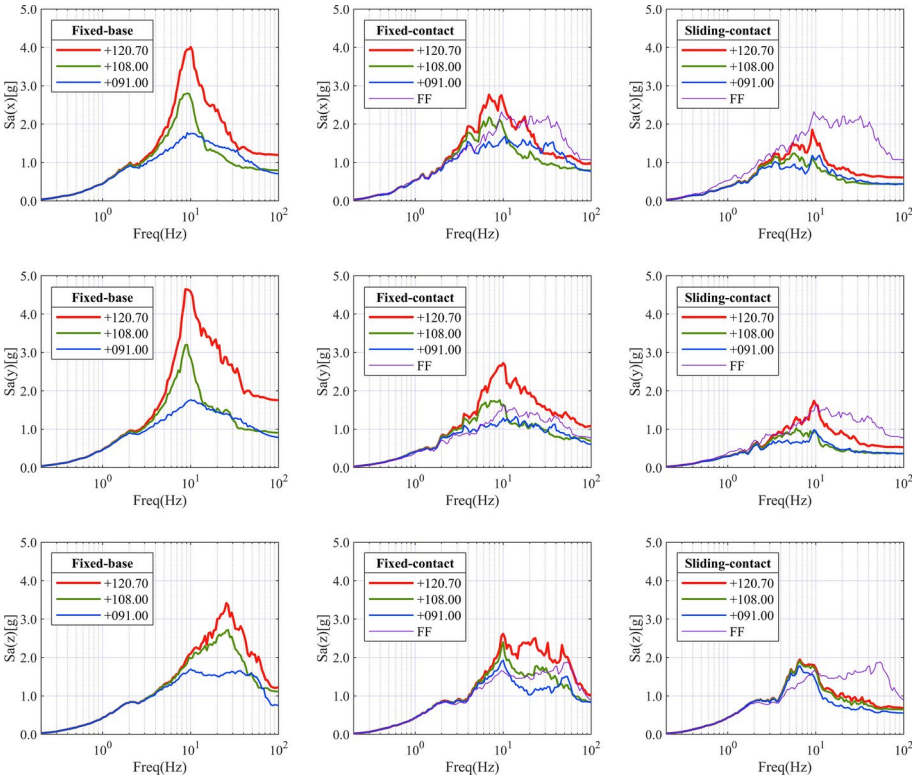

Fig. 14 Floor spectra vs soil-structure contact hypotheses

Table 8 Peak spectral accelerations (PSA) and peak frequencies (f^{PSA})

	Free field		Fixed base		Fixed contact				Sliding contact			
Direction	Surface		Roof		Foundation		Roof		Foundation		Roof	
	f^{PSA}	PSA	f^{PSA}	PSA	f^{PSA}	PSA	f^{PSA}	PSA	f^{PSA}	PSA	f^{PSA}	PSA
Transversal (x)	9.6	2.3	10.0	4.0	10.5	1.7	6.9	2.8	11.0	1.2	9.1	1.9
Longitudinal (y)	10.0	1.6	8.7	4.6	13.9	1.3	10.5	2.7	9.6	1.0	9.6	1.7
Vertical (z)	53.6	1.9	25.4	3.4	10.0	1.9	10.0	2.6	6.6	1.8	6.6	1.9

Table 9 Foundation to free-field PSA ratio (π_{FF})

Direction	Fixed base	Fixed contact	Sliding contact
Transversal (x)	0.77	0.74	0.52
Longitudinal (y)	1.10	0.81	0.63
Vertical (z)	0.89	1.00	0.95

Table 10 Roof to foundation PSA ratio (π_{RF})

Direction	Fixed base	Fixed contact	Sliding contact
Transversal (x)	2.25	1.65	1.58
Longitudinal (y)	2.61	2.08	1.70
Vertical (z)	2.01	1.37	1.06

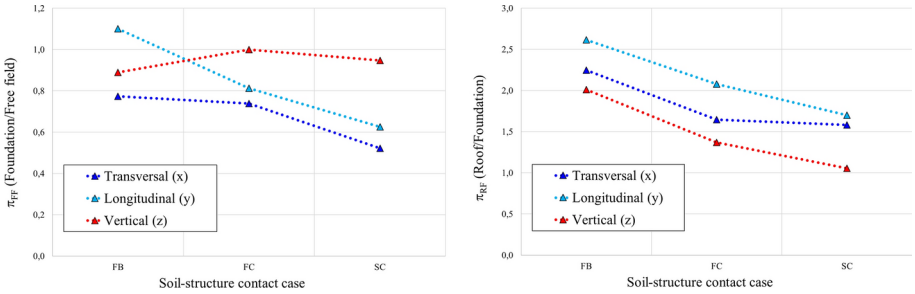

Fig. 15 Evolution of π_{FF} and π_{RF} ratios with the soil-structure contact case

At foundation level, the horizontal floor spectra show a significant and consistent reduction of the PSA in the structure with respect to the free-field response, from the FB to SC cases. The trend is very clear except for the longitudinal direction in the FB case. Vertical floor spectra at the foundation level show a different behavior with a not so clear trend and a slight variation of the free field spectra in terms of PSA.

If the comparison is made among the soil-structure contact cases with respect to the FB case, the horizontal spectra at the foundation level show a significant reduction of the PSA, which increases from the FC case to the SC case. Ratios in the vertical floor spectra show a smaller variation with values around the unity, with PSA values for FC and SC that are slightly higher than in the FB case.

The analysis of the floor spectra at roof level in relation to the soil-structure contact hypotheses show some conclusive results. PSA shows an important amplification effect through the structure for horizontal and vertical components. This amplification consistently decreases from the FB case to the SC case. Note that, the evolution for the three directions is very similar following parallel curves. This leads to the conclusion about the reducing effect on the PSA due to the soil layers underlying the structure and the contact in the interface. Another relevant effect of the soil-structure contact is the variation in the peak frequency. FB shows a f^{PSA} ratio between the roof with respect to base horizontal component of 0.98, which turns into 0.69 in FC case due to the soil influence, and reach a value of 0.92 in the SC due to sliding.

In the case of nuclear structures, special attention should be paid to the systems and components in charge of the correct operation of the entire facility. This operation is highly related to the acting acceleration on the systems and components, which highlights the importance of employing the most advanced technology currently available in terms of modelling and computation. That is, in such structures, it is of utmost importance to provide a reliable estimation of the expected accelerations within the necessary range of frequencies. Accordingly, floor spectra have been obtained at the 46 locations of safety-related systems and components for the three soil-structure contact cases. These points are named with a figure corresponding to the floor and two figures for the order into the floor {102, 204, 506,…}, according to Fig. 13. PSA have been obtained at every point for the three soil-structure contact cases {FB, FC, SC} and, for the three directions {x, y, z}. Results are depicted in Fig. 16, where a vertical segment joins the three PSA obtained at a given point, showing its range of variation.

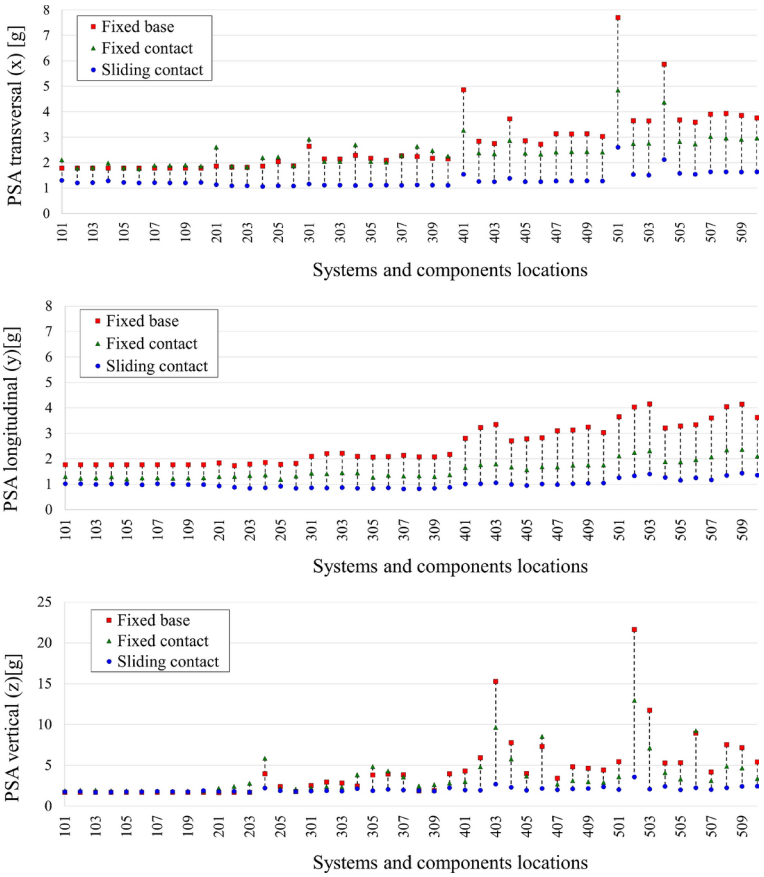

Fig. 16 Range of PSA for the systems and components' locations

Hence, Fig. 16 works as a map of the range of behavior for the floor spectra of the whole set of components. Notice that PSA for a given point does not occur at the same peak frequency. In light of the results, the increasing range of maximum spectral acceleration with the floor can be clearly observed. PSA for the SC case stays around 1 g in the lower levels and increases up to values around 1.5 g at the higher levels close to the roof. However, PSA for FB case shows a fast increase at medium to high levels, reaching values of 4 g or 5 g.

Note that some points in Fig. 16 show an out-of-range behavior and require a deeper analysis. For instance, floor spectra in the transversal direction show a large PSA range for point 501 and, especially, for floor spectra in the vertical direction, three points {403, 502, 503}. The response observed in these points is mainly in the FB case, for which extreme values of PSA are obtained. Yet, the results for the SC case are comparable to those of the adjacent points, which is a clue of the effect of the nonlinearity. Another clue is found at the location of these points on the floor, that is, close to the boundary of the structure adjacent to the containment structure (Fig. 13), where the stiffness of the building is lower. Note that the modal analysis of the structure shows vibration modes with high displacements at this part of the structure that behaves like a cantilever, that is, in a very different way from the

rest of the structure. Furthermore, the mentioned points are placed at the two highest floors. These anomalies with respect to the adjacent points reveal the importance of a detailed study of the local effects and, from a more global point of view, the relevance of considering the nonlinear behavior in the soil-structure interface, which clearly reduces this effect.

6.2 Effect of the uncertainties of the mechanical properties of the soil column

The effect of the uncertainties in the mechanical properties of the soil layers on the floor spectra is addressed herein. As a detailed knowledge of the soil properties is not usually available, a statistical approach has been used to analyze and quantify the effect of the uncertainties of the soil. Figure 17 shows three floor spectra obtained in the structure at the foundation (+91.00) and at the roof (+120.70) in three directions {x, y, z}, for the three columns {LB, BE, UB} described in Sect. 3, and two soil-structure contact cases {FC, SC}. The floor spectra are calculated as the median obtained from the seven seismic ground motions considered in this study. This statistical analysis concerns the stiffness and the

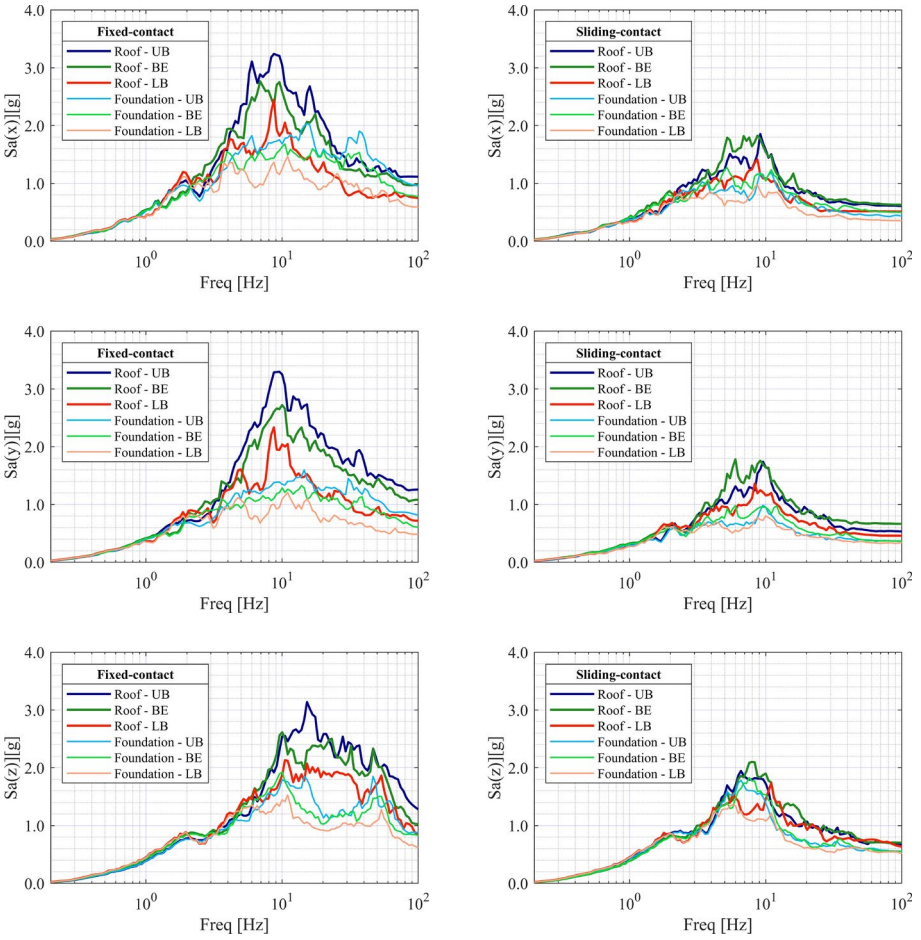

Fig. 17 Floor spectra for three soil columns at foundation and roof levels

Table 11 Peak spectral accelerations (PSA) and range of values vs soil column

	Fixed contact						Sliding contact					
Columns	Foundation			Roof			Foundation			Roof		
	x	y	z	x	y	z	x	y	z	X	y	z
UB	2.03	1.60	1.85	3.24	3.30	3.14	1.19	0.99	1.78	1.85	1.74	1.95
BE	1.68	1.33	1.93	2.77	2.72	2.62	1.27	0.98	1.83	1.82	1.78	2.10
LB	1.46	1.20	1.53	2.45	2.34	2.13	0.97	0.80	1.36	1.41	1.36	1.73
PSA range	0.57	0.40	0.33	0.79	0.96	1.01	0.22	0.18	0.43	0.44	0.38	0.21

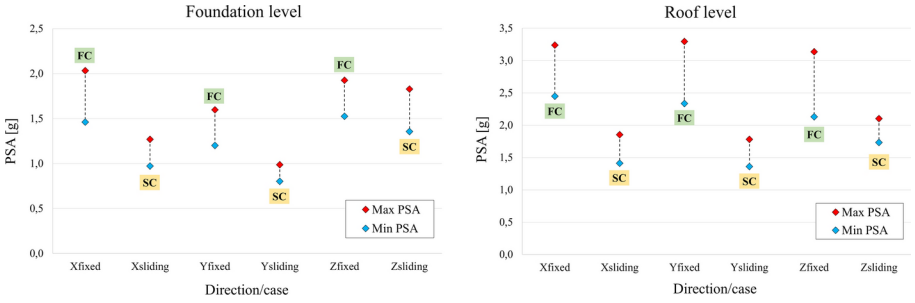

Fig. 18 PSA ranges for floor spectra at foundation and roof level

damping properties of the soil layers. Note that, the evolution of these properties is inverse, thus, UB soil column means a higher stiffness and lower damping, while LB soil column means the opposite; BE column is a median value for both properties.

In the light of this outcome, some conclusions can be extracted. The floor spectra of the nuclear structure observed are very similar in both horizontal directions, but shows some differences in the vertical direction, where significant accelerations appear at high frequencies for the FC case. This widening effect of the range of frequencies is not observed in the SC case. The sliding-rocking at the contact interface produces the flattening of the floor spectra, showing smaller differences in the floor spectra at foundation and roof levels, and among the three soil columns. The effect of the uncertainties of the mechanical properties of the soil column is analyzed in terms of the range of variation observed in the peak spectral acceleration (PSA) of the floor spectra among the three soil columns. To measure this variation, PSA is obtained for each soil-column {LB, BE, UB} and direction {x, y, z} case, at the foundation and roof levels of the structure. A PSA range is calculated as the difference between the maximum and minimum PSA values for the three columns in each case. This PSA range represents a large range of probability of the structural response, and so, it is used as an indicator of the uncertainty. Table 11 shows the PSA obtained for every case {three columns, three directions} and the PSA range for all the cases. Figure 18 shows a scheme of the PSA ranges at the foundation level and at the roof level for every case. Each figure shows the PSA range for the three directions and the two contact cases considered (FC, SC), which allows to compare the whole set of results.

At foundation level, the PSA ranges in the horizontal directions show a significant decrease due to the sliding-rocking at the contact interface, which means a reduction of the uncertainty. The reduction is consistent in both horizontal directions, with ranges of 0.57 and 0.40 for FB case to ranges of 0.18 and 0.22 for the SC case. This effect does not appear

in the vertical component, where the slight reduction of the PSA does not mean a lower range of the PSA.

At roof level, PSA values are higher, consistently with the results described in the previous paragraph, and the PSA ranges between LB and UB columns are also larger for the FC case. However, the reduction in the PSA ranges is also observed in all the directions. In the horizontal directions, ranges evolve from 0.79 and 0.96 without sliding to 0.44 and 0.38 with sliding. In the vertical direction the absolute ranges evolve from 1.01 to 0.21.

7 Conclusions

Depending on the importance of a civil structure (e.g., a nuclear structure), it is necessary to analyze its seismic interaction with the soil using 3D nonlinear models. In this article, an advanced nonlinear soil-structure interaction methodology, for the spectral analysis of a nuclear structure, has been proposed. The starting point has been the determination of the ground motions, the development of the seismic signals that act at the bedrock level and the definition of a detailed 3D numerical model for both soil and structure. All these elements have been integrated to study the effects of the geometric nonlinearities at the soil-structure contact interface and the uncertainty of the multi-layered soil column, on the seismic response of a nuclear structure subjected to *Beyond Design Basis Earthquakes*.

Because of aspects related to both reflection of seismic waves and sampling frequency of accelerograms, calibration of 3D FEM models to meet specific spectral ordinates at the surface is not trivial (Vargas-Alzate et al. 2024). An innovative method has been employed in this research that allows generating accelerograms which, after propagation in the 3D FEM model, produce surface signals whose frequency content coincides with predefined spectral ordinates. In this manner, it has been guaranteed that the input signals at the foundation level of the analyzed structure are in agreement with the expected ground motion, in terms of spectral ordinates, predicted by means of PSHA analysis.

The effects of the nonlinearity on the floor spectra have been analyzed. At foundation level, the floor spectra in horizontal direction show a significant PSA decrease from the fixed base case to the sliding contact case with respect to free field response. However, floor spectra in vertical direction show a smoother decrease in terms of PSA. The reduction of PSA with soil-structure interaction is accentuated when the comparison is made with the floor spectra at the roof level with respect to foundation level, considering the presence of the soil and the relative movements at the soil-structure interface.

The effect of the nonlinearity is also studied by examining the floor spectra in a set of points corresponding to the locations of the safety-related systems and components placed at the floors of the nuclear structure, for three soil-structure contact cases. This analysis confirms and complements the conclusions arisen from the floor spectra in the structure, showing a non-homogenous distribution of the response depending on the floor and the location of the calculation point. The range of PSA between fixed base and sliding contact cases increases with the elevation of the floor. This amplification with the elevation is significantly lower in FC case, while the results for SC case show a stable behavior. Local effects due to the geometry or the local structural behavior can have a strong effect on the floor spectra obtained. This emphasizes the conclusion about the need of considering the

geometric nonlinearity, which is crucial to capture the seismic response at the systems and components' locations.

The effect of the uncertainty of a multi-layered soil column has been studied using a statistical approach by defining three soil-columns that embrace a wide range of probability from 16% (Lower Bound) to 84% (Upper Bound). The soil-structure interaction leads to a significant reduction of the PSA range in the floor spectra with respect to fixed contact case, which means a lower uncertainty in the calculation. This effect is highly significant at roof level in all directions, while at foundation level this reduction in the PSA range is significant only for horizontal directions.

The results presented in this paper suggest that geometric nonlinearities significantly affect to the seismic response of the structure, systems and components of a safety-related nuclear structure and they could potentially have a strong impact on the structural evaluation.

Acknowledgements The authors acknowledge financial support from the Spanish Ministry of Science and Innovation, through the "Severo Ochoa Programme for Centers of Excellence in R&D (2019-2023)" under grant CEX2018-000797-S funded by MCIN/AEI/https://doi.org/10.13039/501100011033.

Funding The authors acknowledge financial support from the Spanish Ministry of Science and Innovation, through the "Severo Ochoa Programme for Centers of Excellence in R&D (2019–2023)" under grant CEX2018-000797-S funded by MCIN/AEI/https://doi.org/10.13039/501100011033.
Open Access funding provided thanks to the CRUE-CSIC agreement with Springer Nature.

Declarations

Conflict of interest The authors declare that they have no known competing financial interests or personal relationships that could have appeared to influence the work reported in this paper.

Open Access This article is licensed under a Creative Commons Attribution 4.0 International License, which permits use, sharing, adaptation, distribution and reproduction in any medium or format, as long as you give appropriate credit to the original author(s) and the source, provide a link to the Creative Commons licence, and indicate if changes were made. The images or other third party material in this article are included in the article's Creative Commons licence, unless indicated otherwise in a credit line to the material. If material is not included in the article's Creative Commons licence and your intended use is not permitted by statutory regulation or exceeds the permitted use, you will need to obtain permission directly from the copyright holder. To view a copy of this licence, visit http://creativecommons.org/licenses/by/4.0/.

References

Abrahamson NA (1992) Non-stationary spectral matching. Seismol Res Lett 63(1):30

Ahn SJ, Park JH (2023) In-structure response spectra of an auxiliary building in a nuclear power plant considering equipment-structure interaction. Appl Sci 13(1):247. https://doi.org/10.3390/app13010247

American Society of Civil Engineers, ASCE. Seismic Analysis of Safety– Related Nuclear Structures. ASCE 4–16. 2017

Barbu LG, Cornejo A, Martínez X, Oller S, Barbat AH (2019) Methodology for the analysis of post-tensioned structures using a constitutive serial-parallel rule of mixtures: large scale non-linear analysis. Compos Struct 216:315–330. https://doi.org/10.1016/j.compstruct.2019.02.092

Bolisetti C, Whittaker AS (2015) Site Response, soil-structure interaction and structure-soil-structure interaction for performance assessment of buildings and nuclear structures. Multidisciplinary center for earthquake engineering research (MCEER). University at Buffalo, NY

Bolisetti C, Whittaker AS, Mason HB, Almufti I, Willford M (2014) Equivalent linear and nonlinear site response analysis for design and risk assessment of safety-related nuclear structures. Nucl Eng Des 275:107–121. https://doi.org/10.1016/j.nucengdes.2014.04.033

Coleman JL, Bolisetti C, Whittaker A (2016) Time-domain soil-structure interaction analysis of nuclear facilities. Nucl Eng Des 298:264–270. https://doi.org/10.1016/j.nucengdes.2015.08.015

Cornejo A, Barbu LG, Escudero C, Martínez X, Oller S, Barbat AH (2018) Methodology for the analysis of post-tensioned structures using a constitutive serial-parallel rule of mixtures. Compos Struct 200:480–497. https://doi.org/10.1016/j.compstruct.2018.05.123

Cornell CA (1968) Engineering seismic risk analysis. Bull Seismol Soc Am 58(5):1583–1606

Datta D, Varma AH, Coleman J (2017) Investigation of interface nonlinearity on soil-structure interaction analyses. Transactions, Structural Mechanics in Reactor Technology, SMiRT-24, Busan, S. Korea.

Davoodi M, Sadjadi M (2015) Assessment of near-field and far-field strong ground motion effects on soil-structure SDOF system. Int J Civ Engrg. 13, 3&4B, Transaction B: Geotechnical Engineering. https://doi.org/10.22068/IJCE.13.3.153

Dawson PR, Boyce D, Eggert G, Bradon A (1995) A consistent penalty method for contact between a deforming viscoplastic workpiece and a rigid tool. Int J Numer Methods Engrg 38:3969–3987. https://doi.org/10.1002/nme.1620382305

Electric Power Research Institute (EPRI). "Seismic Evaluation Guidance - Screening, Prioritization and Implementation Details (SPID) for the Resolution of Fukushima Near-Term Task Force Recommendation 2.1: Seismic". Report 1025287, Palo Alto, CA, February 2013

Fischer KA, Wriggers P (2005) Frictionless 2D contact formulations for finite deformations based on the mortar method. Comput Mech 36:226–244. https://doi.org/10.1007/s00466-005-0660-y

Fischer KA, Wriggers P (2006) Mortar based frictional contact formulation for higher order interpolations using the moving friction cone. Comput Methods Appl Mech Engrg 195:5020–5036. https://doi.org/10.1016/j.cma.2005.09.025

Flores FG, Oñate E (2005) Applications of a rotation-free triangular element for finite strain analysis of thin shells and membranes. Textile composites and inflatable structures. Computational methods in applied sciences springer. vol 3. https://doi.org/10.1007/1-4020-3317-6_5

Galindo M, Oliver J, Cervera M (1993) Simulación numérica del comportamiento no lineal de presas de hormigón ante acciones sísmicas. Monografía CIMNE IS-3. Editor A.H. Barbat. CIMNE.

Hancock J, Watson-Lamprey J, Abrahamson NA, Bommer JJ, Markatis A, McCoy E, Mendis R (2006) An improved method of matching response spectra of recorded earthquake ground motion using wavelets. J Earthquake Eng 10:67–89

Hashash YMA, Musgrove MI, Harmon JA, Ilhan O, Xing G, Numanoglu O, Groholski DR, Phillips CA, Park D (2020) "DEEPSOIL 7, Software". Urbana, IL, Board of Trustees of University of Illinois at Urbana-Champaign.

Hashemi A, Elkhoraibi T, Ostadan F (2015) Effects of structural nonlinearity and foundation sliding on probabilistic response of a nuclear structure. Nucl Eng Des 295:887–900. https://doi.org/10.1016/j.nucengdes.2015.08.028

Jiménez S, Cornejo A, Barbu LG, Barbat AH, Oller S (2021) Failure pressure analysis of a nuclear reactor prestressed concrete containment building. Eng Struct 236:112052. https://doi.org/10.1016/j.engstruct.2021.112052

Kaklamanos J, Bradley BA, Thompson EM (2013) Baise LG (2013) Critical parameters affecting bias and variability in site-response analyses using KiK-net downhole array data. Bull Seismol Soc Am 103(3):1733–1749. https://doi.org/10.1785/0120120166

Koo YH, Yang YS, Song KW (2014) Radioactivity release from the Fukushima accident and its consequences: a review. Prog Nucl Energy 74:61–70. https://doi.org/10.1016/j.pnucene.2014.02.013

Martinez X, Rastellini F, Oller S, Flores F, Oñate E (2011) Computationally optimized formulation for the simulation of composite materials and delamination failures. Compos B Engrg 42(2):134–144. https://doi.org/10.1016/j.compositesb.2010.09.013

NUREG/CR-6728 (2001), Technical basis for revision of regulatory guidance on design ground motions: hazard- and risk-consistent ground motion spectra guidelines. Risk engineering, Inc. U.S. nuclear regulatory commission office of nuclear regulatory research Washington, DC 20555–0001

Oliver J, Hartmann S, Cante JC, Weyler R, Hernández J (2009) A contact domain method for large deformation frictional contact problems. Part 1: theoretical basis. Comput Methods Appl Mech Engrg 198:2591–2606. https://doi.org/10.1016/j.cma.2009.03.006

Poul MK, Zerva A (2018) Efficient time-domain deconvolution of seismic ground motions using the equivalent-linear method for soil-structure interaction analyses. Soil Dyn Earthq Eng 112:138–151. https://doi.org/10.1016/j.soildyn.2018.04.032

Rastellini FG, Oller S, Salomon O, Oñate E (2008) Composite materials non-linear modeling for long fiber-reinforced laminates: continuum basis, computational aspects and validations. Comput Struct 86(9):879–896. https://doi.org/10.1016/j.compstruc.2007.04.009

Seed H. B. and Idriss I. M. (1970) "Soil Moduli and damping factors for dynamic response analyses". Report No. EERC 70–10, Earthq. Research Center, Univ. California Berkley.

Toro GR (1996) Probabilistic models of site velocity profiles for generic and site-specific ground motion amplification studies. Report submitted to Brookhaven National Laboratory, Upton, New York.
US NRC "A performance-based approach to define the site-specific earthquake ground motion" Regulatory guide RG 1.208, March 2007
US NRC standard review plan for the review of safety analysis reports for nuclear power plants: LWR edition / Chapter 3.7.1 Seismic design parameters. NUREG-0800, Washington, DC, December 2014.
US NRC "Seismic design classification for nuclear power plants" Regulatory guide 1.29, revision 6. July 2021.
Vargas-Alzate Y, Barbat AH, Pujades L, Pinzón L, Gonzalez JM, Ramirez J, Rastellini F (2024) Characterization of free-field seismic motions for soil-structure interaction analysis of nuclear structures using enhanced transfer functions. Soil Dyn Earthq Eng 179:108494. https://doi.org/10.1016/j.soildyn.2024.108494
Weyler R, Oliver J, Sain T, Cante JC (2012) On the contact domain method: a comparison of penalty and Lagrange multiplier implementations. Comput Methods Appl Mech Engrg 205–208:68–82. https://doi.org/10.1016/j.cma.2011.01.011
Yoshida N, Kobayashi S, Suetomi I, Miura K (2002) Equivalent linear method considering frequency dependent characteristics of stiffness and damping. Soil Dyn Earthq Eng 22(3):205–222. https://doi.org/10.1016/S0267-7261(02)00011-8

Publisher's Note Springer Nature remains neutral with regard to jurisdictional claims in published maps and institutional affiliations.

Authors and Affiliations

J. M. Gonzalez[1,2] · A. H. Barbat[1,2] · Y. F. Vargas-Alzate[1] · F. Rastellini[1,2] · J. Ramirez[1,2] · C. Escudero[2] · L. G. Pujades[1]

✉ J. M. Gonzalez
jose.manuel.gonzalez@upc.edu

A. H. Barbat
alex.barbat@upc.edu

Y. F. Vargas-Alzate
yeudy.felipe.vargas@upc.edu

F. Rastellini
frastellini@cimne.upc.edu

J. Ramirez
jramirez@cimne.upc.edu

C. Escudero
cuauhtemoc@cimne.upc.edu

L. G. Pujades
lluis.pujades@upc.edu

[1] Department of Civil and Environmental Engineering (DECA), Universitat Politècnica de Catalunya - Barcelona Tech (UPC), Jordi Girona 1-3 08034, Barcelona, Spain

[2] Centre Internacional de Mètodes Numèrics en Enginyeria (CIMNE), Gran Capitan S/N, 08034 Barcelona, Spain